3-1993

Doubly Differential Electron-Production Cross Sections for 200- 1500-eV e^- +H_2 Collisions

M. Eugene Rudd
University of Nebraska - Lincoln, erudd@unl.edu

K. W. Hollman
University of Nebraska - Lincoln

J. K. Lewis
University of Nebraska - Lincoln

D. L. Johnson
University of Nebraska - Lincoln

R. R. Porter
University of Nebraska - Lincoln

See next page for additional authors

Doubly differential electron-production cross sections for 200–1500-eV $e^- + H_2$ collisions

M. E. Rudd, K. W. Hollman, J. K. Lewis, D. L. Johnson, R. R. Porter, and E. L. Fagerquist
Department of Physics and Astronomy, University of Nebraska-Lincoln, Lincoln, Nebraska 68588-0111
(Received 8 September 1992)

Ionization cross sections differential in the angle and energy of the detected electrons were measured for electron impact on hydrogen gas at 200, 500, 1000, and 1500 eV. Measurements were made from 15°–150° and from a few eV to $T-I$ where T is the primary electron energy and I the ionization potential of hydrogen. The results are compared to earlier measurements and to available calculations.

PACS number(s): 34.80.Dp

I. INTRODUCTION

One of the most fundamental and ubiquitous processes occurring in nature is the collision of an electron with an atom or molecule. An important process resulting from such collisions is ionization, with the ensuing loss of energy and change of direction of the primary electron and the emission of one or more secondary electrons. Knowledge of this process has numerous applications in such areas as studies of the aurora, stellar atmospheres, radiation damage, particle detector operation, and in various processes involving ionized gases or plasmas.

Early measurements of integral or total cross sections (TCS's) for electron-impact ionization have been supplemented in recent years by determinations of doubly differential cross sections (DDCS's), i.e, measurements of the angular and energy distributions of the electrons emitted. While a considerable body of data for helium gas targets has accumulated, the only measurements on hydrogen gas have been by Opal, Peterson, and Beaty [1] at 500 eV, Shyn, Sharp, and Kim [2] at several energies from 25 to 250 eV, and DuBois and Rudd [3] at 100 eV. No DDCS data is available for hydrogen at energies above 500 eV. The detected energies in the data of Shyn, Sharp, and Kim and Opal, Peterson, and Beaty extended only up to the lower of 200 eV or $(T-I)/2$, where T is the primary energy and I the ionization potential of molecular hydrogen (15.4 eV), while that of DuBois and Rudd extended to $(T-I)$, as do the present measurements.

By integrating the DDCS over angle, one obtains the singly differential cross section (SDCS):

$$\sigma(W)=2\pi\int_0^{\pi}\sigma(W,\theta)\sin\theta\, d\theta \ . \tag{1}$$

A further integration over ejection energy yields the TCS for ionization:

$$\sigma_{\rm ion}=\tfrac{1}{2}\int_0^{T-I}\sigma(W)\, dW \ . \tag{2}$$

The factor $\frac{1}{2}$ accounts for the fact that there are two electrons from each ionizing collision, the secondary electron and the scattered primary electron.

Absolute cross-section measurements, especially the DDCS's, provide a basis for testing theoretical models and semiempirical descriptions of ionization. Because of difficulties in obtaining wave functions for molecular targets, no quantum-mechanical calculations are known for electron–molecular-hydrogen ionization, so we will use the classical binary-encounter approximation (BEA) and a semiempirical model to provide analytical representations of the cross sections.

II. BINARY-ENCOUNTER APPROXIMATION

Several versions of the classical BEA are available in the literature. We will use the symmetrical model given by Vriens [4] with his energy transfer E equal to $W+I$, where W is the ejected-electron energy, his initial target energy E_2 equal to I, and his parameter ϕ equal to unity. Written in terms of the dimensionless variables $w=W/I$ and $t=T/I$, the SDCS is given by

$$\sigma(w)=\frac{S}{I(t+2)}\left[\frac{1}{(w+1)^2}+\frac{4}{3(w+1)^3}+\frac{1}{(t-w)^2}+\frac{4}{3(t-w)^3}-\frac{1}{(w+1)(t-w)}\right], \tag{3}$$

where $S=4\pi a_0^2 N(R/I)^2$, with a_0 being the Bohr radius, N the number of electrons in the target, and R the Rydberg energy (13.6 eV). The TCS in the BEA is

$$\sigma_{\rm ion}=\frac{S}{t+2}\left[\frac{5}{3}-\frac{1}{t}-\frac{2}{3t^2}-\frac{\ln t}{t+1}\right] . \tag{4}$$

III. SEMIEMPIRICAL MODEL

The semiempirical model of Rudd [5] provides another convenient analytical representation of the SDCS and TCS and in addition yields the DDCS. In this model the SDCS is given by

$$\sigma(w,t)=SF(t)f_1(w,t)/I \ , \tag{5}$$

where

$$f_1(w,t)=\frac{1}{(w+1)^n}+\frac{1}{(t-w)^n}-\frac{1}{[(w+1)(t-w)]^{n/2}} \tag{6}$$

with $n=2.4$. The expression

$$F(t)=\frac{A_1 \ln t}{t}+\frac{A_2}{t+A_4}+\frac{A_3}{t^2} \tag{7}$$

has been modified slightly from that in Ref. [5] to give somewhat better agreement with the experimental TCS. The parameters $A_1,\ldots,A_4$ have values 0.55, 1.73, -0.14, and 2.9, respectively, for the best fit to the hydrogen TCS data.

In this model the DDCS is given by

$$\sigma(w,t,\theta)=G_1[f_{\mathrm{BE}}(w,t,\theta)+G_4 f_b(w,t,\theta)] , \tag{8}$$

where

$$f_{\mathrm{BE}}(w,t,\theta)=\frac{1}{1+[(\cos\theta-G_2)/G_3]^2} \tag{9}$$

represents the binary-encounter peak and

$$f_b(w,t,\theta)=\frac{1}{1+[(\cos\theta+1)/G_5]^2} \tag{10}$$

describes the rise in the cross sections in the backward direction which is seen in some data. The value of G_5 is 0.33. The other parameters are

$$G_1=\frac{SF(t)f_1(w,t)/I}{g_{\mathrm{BE}}(w,t)+G_4 g_b(w,t)} , \tag{11}$$

$$G_2=\cos\theta_0=\left[\frac{w+1}{t}\right]^{1/2} , \tag{12}$$

$$G_3=\beta\left[\frac{1-G_2^2}{w}\right]^{1/2} , \tag{13}$$

$$G_4=\gamma\frac{(1-w/t)^3}{t(w+1)} , \tag{14}$$

with

$$g_{\mathrm{BE}}=\int f_{\mathrm{BE}}(w,t,\theta)d\Omega$$

$$=2\pi G_3\left[\tan^{-1}\left[\frac{1-G_2}{G_3}\right]+\tan^{-1}\left[\frac{1+G_2}{G_3}\right]\right] , \tag{15}$$

$$g_b=\int f_b(w,t,\theta)d\Omega$$

$$=2\pi G_5\tan^{-1}(2/G_5)=2.9 , \tag{16}$$

and with $\gamma=10$ and $\beta=0.60$. The TCS for ionization is given by

$$\sigma_{\mathrm{ion}}=SF(t)g_1(t) , \tag{17}$$

where

$$g_1(t)=\frac{1-t^{1-n}}{n-1}-\left[\frac{2}{t+1}\right]^{n/2}\frac{1-t^{1-n/2}}{n-2} . \tag{18}$$

Although the asymptotic primary-electron energy dependence in this model has been chosen to match the well-verified Bethe $(\ln t)/t$ relation, neither this representation nor the BEA specifically includes the dipole interaction. However, for simple gases such as hydrogen and helium the dipole contribution is small.

IV. APPARATUS AND EXPERIMENTAL METHOD

With minor improvements the apparatus used to take the data is the same as that employed in earlier work [3,6–9], which may be consulted for further details. A rotatable electron gun with a thoriated filament as a cathode and an einzel lens produces a finely collimated electron beam. A shielded suppressor in the gun prevents low-energy electrons emitted at the defining apertures from entering the collision region. A static gas target [at a pressure typically of $(3-8)\times10^{-4}$ Torr] fills the chamber. Electrons, both secondary and scattered primary, from a short length of beam are selected by a collimator and enter a parallel-plate electrostatic analyzer with a resolution of 1.1%. The angular range covered is 15°–150° relative to the primary beam. The analyzer, channeltron detector, and electron gun are enclosed and differentially pumped. While the pressure in the analyzer cannot be measured directly, it is estimated to be about $(2-3)\times10^{-6}$ Torr while target gas is present. The base pressure in the chamber without target gas is about 10^{-6} Torr. A slit held at one-half the analyzer back-plate potential is placed between the exit slit of the analyzer and the cone of the channeltron to reduce spurious low-energy electrons, which are troublesome at small angles [9]. Magnetic shielding in the chamber surrounds the collision region as well as the analyzer and electron gun. Some stainless-steel screws, which were found to be magnetic, were replaced.

The Faraday cup used in the 1500-eV measurements had a rather large aperture relative to its depth and was responsible for a high background in those measurements. This was replaced for the other measurements by a deeper and narrower cup. The target-gas density was determined from measurements of the temperature and the pressure, the latter being read by a capacitance manometer.

Because there were large statistical fluctuations in regions of the spectra where the count rate was very low, in many cases we have averaged the cross sections from several runs to obtain smoother curves. It is difficult to state uncertainties since they vary considerably with primary- and secondary-electron energy and angle and sometimes there are unexplained variations from run to run. A reasonable estimate for the uncertainty in the DDCS's is 30% and for the SDCS's 25% although it may be much higher at low secondary energies and near $W=(T-I)/2$ where the cross sections are generally very small. As $W\rightarrow T-I$ the measured SDCS's fall below the expected values because the angular region below 15° is not measured. This problem was discussed previously [9].

V. EXPERIMENTAL RESULTS

Tables I–IV give samples of the DDCS's and SDCS's. At the two higher energies the binary peaks are so sharp that with the relatively coarse angular mesh used the

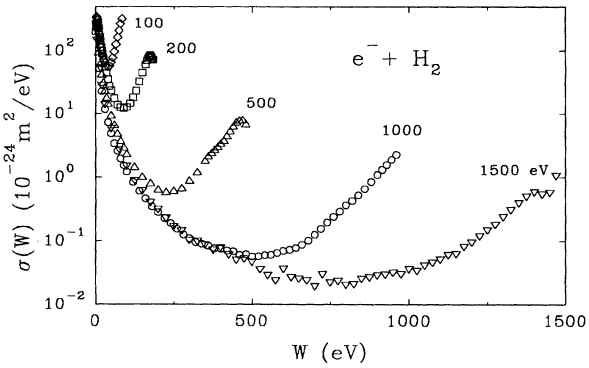

FIG. 1. Singly differential cross sections (SDCS's) for electron production in molecular hydrogen by electrons of 100, 200, 500, 1000, and 1500 eV primary-electron energies. The 100-eV data are from DuBois and Rudd [3].

SDCS's obtained by numerical integration over angle resulted in a spectrum with a series of bumps, one for each measured angle. To smooth out the SDCS's to give a truer electron spectrum we have used the semiempirical model to interpolate between some of the measured angles. Some evidence of this problem is visible near the high-energy end of the 500-eV data in Figs. 1 and 2, since this corrective procedure was not applied to that set of data.

TCS's could have been obtained by integration of the SDCS's, but because the experimental uncertainties are large at the low energies that contribute most to the integral, the results would not be useful. The TCS's have been measured with greater accuracy by other methods; see, e.g., Ref. [10].

The SDCS's are shown in Fig. 1 for the four energies measured and also for 100-eV primary electrons using the data of DuBois and Rudd [3]. Equations (5) and (17) of the semiempirical model yield

$$\frac{I\sigma(w,t)}{\sigma_{\rm ion}} = \frac{f_1(w,t)}{g_1(t)} \ . \tag{19}$$

For $w \ll t$ and $t \gg 1$,

$$\frac{I\sigma(w,t)}{\sigma_{\rm ion}} = \frac{n-1}{(w+1)^n} \ . \tag{20}$$

Then, for large primary- and small secondary-electron energies, a log-log plot of $I\sigma(w,t)/\sigma_{\rm ion}$ vs $w+1$ should

TABLE I. DDCS's for ejection of electrons from H_2 by 200-eV electrons in units of 10^{-24} m^2/eV sr and SDCS's in units of 10^{-24} m^2/eV. Numbers in square brackets are powers of 10 by which the preceding number is to be multiplied. Angle in degrees given at the head of each column.

W (eV)	15°	20°	30°	35°	40°	50°	60°
5	4.12[1]	3.39[1]	2.79[1]	2.85[1]	3.19[1]	3.08[1]	3.46[1]
10	1.79[1]	1.59[1]	1.64[1]	1.75[1]	2.03[1]	2.10[1]	2.39[1]
15	7.60[0]	7.48[0]	9.54[0]	8.94[0]	1.15[1]	1.33[1]	1.58[1]
20	4.83[0]	4.96[0]	5.59[0]	6.46[0]	7.78[0]	9.55[0]	1.22[1]
30	2.31[0]	2.52[0]	2.69[0]	3.77[0]	4.66[0]	5.99[0]	7.86[0]
40	1.32[0]	1.47[0]	2.00[0]	2.49[0]	3.28[0]	4.59[0]	5.69[0]
50	9.48[−1]	1.17[0]	1.53[0]	1.82[0]	2.87[0]	3.63[0]	3.75[0]
60	9.77[−1]	1.18[0]	1.43[0]	1.66[0]	2.69[0]	3.13[0]	2.92[0]
80	1.88[0]	1.44[0]	1.97[0]	2.02[0]	3.20[0]	2.51[0]	1.68[0]
100	4.43[0]	2.74[0]	3.17[0]	3.17[0]	4.19[0]	1.98[0]	9.46[−1]
120	1.20[1]	6.95[0]	5.98[0]	5.09[0]	4.46[0]	1.60[0]	6.77[−1]
140	4.02[1]	1.92[1]	1.09[1]	6.40[0]	3.65[0]	1.31[0]	6.90[−1]
160	1.82[2]	5.11[1]	1.28[1]	6.19[0]	2.96[0]	1.58[0]	8.56[−1]
180	5.87[2]	8.11[1]	1.13[1]	6.33[0]	3.70[0]	1.93[0]	1.18[0]

W (eV)	70°	80°	90°	110°	130°	150°	SDCS
5	3.41[1]	3.19[1]	3.09[1]	2.18[1]	3.06[1]	2.26[1]	3.40[2]
10	2.61[1]	2.40[1]	1.92[1]	1.21[1]	2.02[1]	1.40[1]	2.19[2]
15	1.62[1]	1.51[1]	1.25[1]	7.42[0]	1.21[1]	8.50[0]	1.36[2]
20	1.18[1]	1.11[1]	7.82[0]	4.23[0]	8.16[0]	5.53[0]	9.22[1]
30	6.92[0]	5.64[0]	3.54[0]	1.50[0]	4.33[0]	2.71[0]	4.89[1]
40	4.47[0]	3.11[0]	1.78[0]	6.28[−1]	2.80[0]	1.51[0]	3.09[1]
50	2.61[0]	1.67[0]	1.04[0]	3.59[−1]	2.02[0]	9.78[−1]	2.05[1]
60	1.72[0]	1.02[0]	5.08[−1]	2.36[−1]	1.71[0]	6.70[−1]	1.57[1]
80	8.14[−1]	4.67[−1]	2.63[−1]	1.05[−1]	1.88[0]	6.37[−1]	1.29[1]
100	4.88[−1]	2.95[−1]	1.92[−1]	7.53[−2]	2.55[0]	8.87[−1]	1.43[1]
120	4.11[−1]	2.66[−1]	2.10[−1]	5.52[−2]	3.57[0]	1.38[0]	1.92[1]
140	4.48[−1]	3.64[−1]	2.51[−1]	8.30[−2]	4.96[0]	1.73[0]	2.92[1]
160	5.51[−1]	5.20[−1]	4.01[−1]	1.01[−1]	5.44[0]	1.75[0]	5.02[1]
180	8.97[−1]	6.14[−1]	4.98[−1]	2.04[−1]	5.22[0]	1.83[0]	8.84[1]

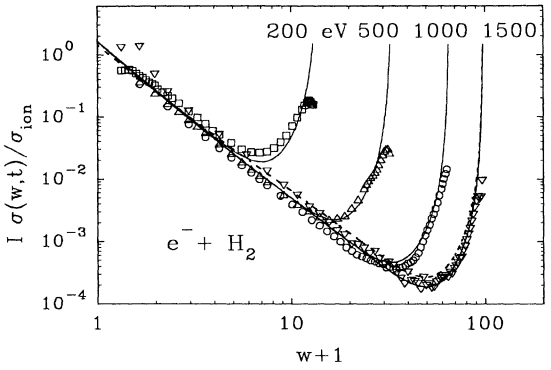

FIG. 2. SDCS's plotted as a ratio to the total cross section (TCS) and multiplied by the ionization potential I. Plotted in this way on a log-log scale, a universal straight line results for large primary- and small secondary-electron energies which may be used to judge the accuracy of experimental data. See text. Solid lines, calculations from the semiempirical model using Eq. (19); dashed line, the binary encounter approximation (BEA) calculated from Eqs. (3) and (4) for 1500 eV.

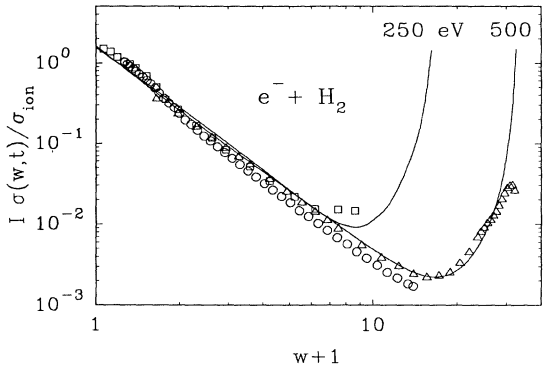

FIG. 3. Graph similar to Fig. 2. △, present 500-eV data; ○, 500-eV data of Opal, Peterson, and Beaty [1]; □, 250-eV data of Shyn, Sharp, and Kim [2]; ——, calculations from Eq. (19).

be a universal straight line with a slope of $-n$ and an intercept (at $w=0$) of $n-1$. The graphs of the SDCS's plotted this way are shown in Fig. 2 along with the results of the model using $n=2.4$. The data follow the expected behavior fairly closely. The BEA results for $T=1500$ eV derived from Eqs. (3) and (4) are plotted as

TABLE II. Same as Table I for 500-eV electrons.

W (eV)	15°	20°	30°	40°	50°	60°	70°
10	1.02[1]	7.85[0]	6.93[0]	8.64[0]	9.58[0]	1.13[1]	1.18[1]
15	4.71[0]	4.48[0]	3.79[0]	5.22[0]	5.96[0]	7.67[0]	7.81[0]
20	2.90[0]	2.08[0]	2.29[0]	3.29[0]	4.26[0]	5.28[0]	5.77[0]
30	1.42[0]	1.20[0]	1.20[0]	1.68[0]	2.29[0]	3.35[0]	3.79[0]
40	6.26[−1]	4.22[−1]	6.81[−1]	9.82[−1]	1.54[0]	2.31[0]	2.71[0]
60	1.72[−1]	2.28[−1]	2.48[−1]	4.47[−1]	7.48[−1]	1.35[0]	1.39[0]
80	1.68[−1]	1.54[−1]	1.21[−1]	2.67[−1]	5.57[−1]	9.58[−1]	8.87[−1]
100	5.82[−2]	1.09[−1]	8.49[−2]	1.83[−1]	4.25[−1]	7.24[−1]	5.07[−1]
150	6.47[−2]	3.77[−2]	5.60[−2]	1.34[−1]	3.25[−1]	3.58[−1]	1.24[−1]
200	5.83[−2]	4.35[−2]	7.51[−2]	1.71[−1]	2.99[−1]	1.31[−1]	3.78[−2]
250	1.08[−1]	9.89[−2]	1.80[−1]	3.11[−1]	1.79[−1]	5.02[−2]	1.78[−2]
300	2.67[−1]	2.39[−1]	6.17[−1]	4.37[−1]	8.93[−2]	3.11[−2]	1.49[−2]
350	8.77[−1]	7.93[−1]	2.14[0]	3.13[−1]	6.88[−2]	3.89[−2]	1.60[−2]
400	4.85[0]	4.19[0]	2.65[0]	2.05[−1]	8.52[−2]	5.25[−2]	3.20[−2]
450	3.68[1]	1.22[1]	1.03[0]	3.57[−1]	1.95[−1]	1.24[−1]	6.88[−2]

W (eV)	80°	90°	110°	130°	150°	SDCS
10	1.21[1]	1.09[1]	7.57[0]	3.15[0]	8.72[−1]	9.61[1]
15	7.86[0]	7.22[0]	5.02[0]	2.31[0]	6.14[−1]	6.26[1]
20	5.89[0]	4.89[0]	3.44[0]	1.38[0]	4.10[−1]	4.29[1]
30	3.30[0]	2.53[0]	1.59[0]	6.97[−1]	2.73[−1]	2.36[1]
40	2.29[0]	1.45[0]	7.95[−1]	3.73[−1]	1.89[−1]	1.47[1]
60	9.79[−1]	5.55[−1]	2.56[−1]	1.43[−1]	9.07[−2]	6.66[0]
80	4.32[−1]	2.20[−1]	1.01[−1]	6.17[−2]	5.01[−2]	3.77[0]
100	2.32[−1]	9.41[−2]	4.08[−2]	4.08[−2]	3.45[−2]	2.35[0]
150	4.84[−2]	3.09[−2]	1.18[−2]	1.09[−2]	1.25[−2]	1.03[0]
200	1.97[−2]	8.29[−3]	4.61[−3]	5.30[−3]	8.12[−3]	6.50[−1]
250	1.02[−2]	9.73[−3]	4.60[−3]	4.57[−3]	4.57[−3]	6.16[−1]
300	8.85[−3]	6.10[−3]	2.71[−3]	3.88[−3]	3.32[−3]	8.86[−1]
350	1.53[−2]	1.04[−2]	3.59[−2]	5.99[−3]	2.60[−3]	1.84[0]
400	1.88[−2]	1.75[−2]	6.55[−2]	8.15[−3]	5.43[−3]	3.35[0]
450	4.72[−2]	4.50[−2]	1.31[−2]	1.98[−2]	1.06[−2]	7.40[0]

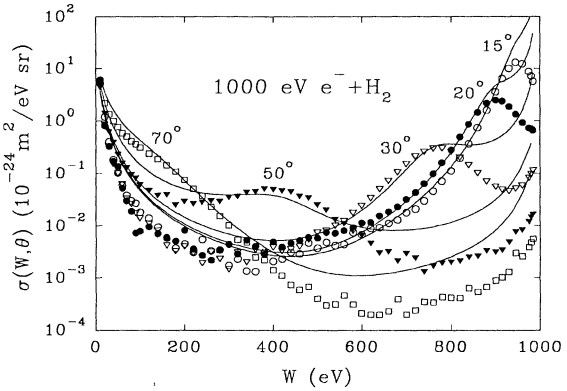

FIG. 4. DDCS's for electrons at the forward angles for 1000-eV primary electrons. —— calculations from Eq. (8).

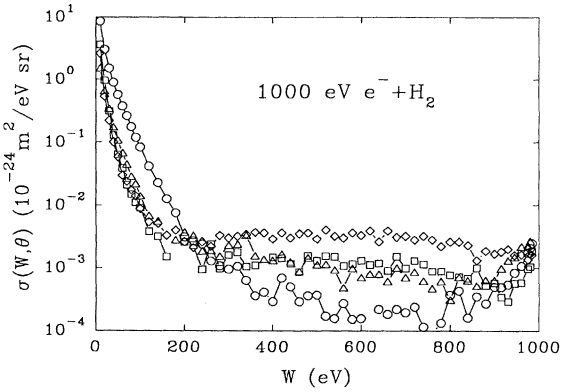

FIG. 5. DDCS's for electrons at the backward angles for 1000-eV primary electrons. ○, 90°; △, 110°; □, 130°; ◇, 150°.

the dashed line. For small and large values of W the results of the BEA are nearly indistinguishable from those of the semiempirical model, but for intermediate values of W (near the minimum) the BEA results are somewhat higher than the model, with the data laying between the two. In Fig. 3 the present 500-eV SDCS data are compared to those of Opal, Peterson, and Beaty [1] and to the predictions of the semiempirical model. The 250-eV data of Shyn, Sharp, and Kim [2] are also plotted. The data of Shyn, Sharp, and Kim [2] and Opal, Peterson, and Beaty

TABLE III. Same as Table I for 1000-eV electrons.

W (eV)	15°	20°	30°	50°	70°
10	5.39[0]	6.11[0]	4.46[0]	4.74[0]	5.69[0]
20	1.19[0]	8.14[−1]	8.54[−1]	1.39[0]	2.22[0]
30	3.97[−1]	3.16[−1]	3.26[−1]	6.17[−1]	1.34[0]
50	1.04[−1]	1.36[−1]	1.00[−1]	2.26[−1]	7.61[−1]
70	3.78[−2]	2.99[−2]	3.32[−2]	1.28[−1]	5.04[−1]
100	1.81[−2]	7.86[−3]	1.40[−2]	6.03[−2]	3.09[−1]
140	9.46[−3]	7.07[−3]	8.12[−3]	3.79[−2]	1.89[−1]
200	4.48[−3]	8.24[−3]	3.96[−3]	2.89[−2]	7.48[−2]
240	5.38[−3]	2.74[−3]	1.91[−3]	2.83[−2]	3.69[−2]
300	1.73[−3]	4.44[−3]	1.46[−3]	3.49[−2]	1.02[−2]
400	2.08[−3]	4.86[−3]	3.88[−3]	4.93[−2]	1.43[−3]
500	3.67[−3]	5.82[−3]	7.44[−3]	2.48[−2]	3.97[−4]
600	6.84[−3]	1.13[−2]	2.41[−2]	6.46[−3]	2.06[−4]
700	1.80[−2]	3.24[−2]	1.52[−1]	2.94[−3]	2.00[−4]
800	1.13[−1]	2.76[−1]	2.63[−1]	2.01[−3]	4.15[−4]
900	3.57[0]	2.53[0]	5.65[−2]	3.15[−3]	8.93[−4]

W (eV)	90°	110°	130°	150°	SDCS
10	8.55[0]		3.62[0]	2.56[0]	5.23[1]
20	3.00[0]	1.51[0]	9.59[−1]	5.33[−1]	2.27[1]
30	1.50[0]	6.46[−1]	3.11[−1]	2.16[−1]	1.17[1]
50	5.73[−1]	1.75[−1]	6.41[−2]	5.89[−2]	4.86[0]
70	2.59[−1]	6.80[−2]	2.12[−2]	2.42[−2]	2.57[0]
100	8.44[−2]	2.17[−2]	9.14[−3]	8.82[−3]	1.22[0]
140	2.28[−2]	6.84[−3]	3.20[−3]	5.11[−3]	6.05[−1]
200	3.15[−3]	2.76[−3]	2.59[−3]	2.62[−3]	2.81[−1]
240	2.36[−3]	3.33[−3]	9.39[−4]	2.64[−3]	1.89[−1]
300	9.48[−4]	1.55[−3]	1.60[−3]	3.02[−3]	1.09[−1]
400	2.94[−4]	1.37[−3]	1.48[−3]	2.89[−3]	7.51[−2]
500	3.69[−4]	1.45[−3]	1.31[−3]	2.94[−3]	5.71[−2]
600	1.55[−4]	9.76[−4]	1.30[−3]	3.34[−3]	7.01[−2]
700	1.94[−4]	1.01[−3]	9.83[−4]	3.15[−3]	1.26[−1]
800	3.70[−4]	6.06[−4]	7.67[−4]	2.57[−3]	3.63[−1]
900	4.97[−4]	6.42[−4]	5.77[−4]	1.69[−3]	1.09[0]

[1] drop noticeably at about $w+1=1.8$, a tendency not seen in any of our data. Nevertheless, the agreement among the three experimental results and the semiempirical model is within the uncertainties.

The DDCS data for 1000-eV primary energy are displayed in Fig. 4 for the forward angles along with the results of the semiempirical model from Eq. (8). The binary peaks, which appear at the energies given by Eq. (12), are reasonably well represented by the model but the cross sections above and below the peaks are often overestimated. Figure 5 shows the data for the backward hemisphere where for secondary-electron energies above 200 eV there is a marked increase in the cross sections with increasing angle which is not matched well by the model, even with a radical readjustment of the parameters. This results in a sudden change in the slope of the curves, which leads to the suspicion that there is a background of spurious electrons. In that energy and angular region the cross section is 3–5 orders of magnitude smaller than that for low-energy electrons or for primary electrons which are scattered elastically or with a small loss of energy. If only a small fraction of the much more numerous slow or fast electrons are able to reach the detector when the analyzer is set for the intermediate energies in question, that would explain this effect. Therefore it is believed that this measured rise at large angles is spurious. However, since none of the previous measurements [1–3] in hydrogen and very few of the measure-

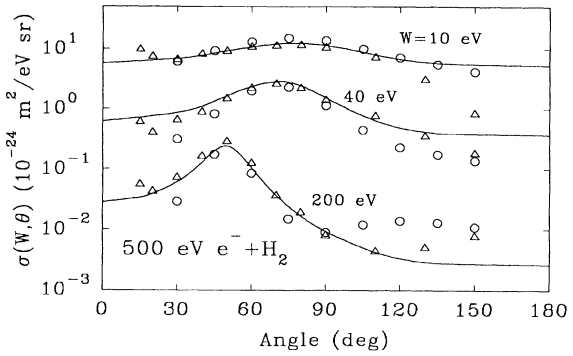

FIG. 6. Angular distributions of the DDCS's for 10-, 40-, and 200-eV electrons from 500-eV collisions. ○, data of Opal, Peterson, and Beaty [1]; △, present data; ——, calculations from Eq. (8).

TABLE IV. Same as Table I for 1500-eV electrons.

W (eV)	15°	20°	30°	40°	50°	60°	70°
10		2.04[0]	3.61[0]	1.05[1]	2.33[1]	1.17[1]	9.15[0]
15	1.60[1]	1.06[0]	1.16[0]	4.70[0]	8.82[0]	7.05[0]	5.56[0]
20	4.53[0]	5.92[−1]	6.45[−1]	1.95[0]	4.31[0]	4.31[0]	3.51[0]
30	6.20[−1]	2.44[−1]	2.64[−1]	6.01[−1]	1.63[0]	2.25[0]	1.67[0]
50	1.38[−1]	5.72[−2]	6.85[−2]	1.76[−1]	3.87[−1]	9.01[−1]	6.73[−1]
100	2.36[−2]	1.98[−2]	1.81[−2]	3.36[−2]	6.00[−2]	2.42[−1]	2.33[−1]
200	5.75[−3]	4.84[−3]	4.03[−3]	7.59[−3]	8.26[−3]	9.44[−2]	9.84[−2]
300	1.92[−3]	2.05[−3]	1.28[−3]		8.79[−3]	7.07[−2]	2.58[−2]
500	2.78[−3]	1.62[−3]	2.48[−3]	3.82[−3]	1.30[−2]	3.15[−2]	3.24[−3]
700	3.44[−3]	9.31[−4]	2.80[−3]	6.45[−3]	1.44[−2]		1.13[−3]
900	4.45[−3]	2.88[−3]	5.41[−3]	2.39[−2]	2.66[−3]	2.65[−3]	1.71[−3]
1000	6.52[−3]	4.65[−3]	1.61[−2]	1.54[−2]	3.21[−3]	8.88[−4]	
1100	1.26[−2]	1.07[−2]	6.79[−2]	6.54[−3]	2.12[−3]	2.72[−3]	1.54[−3]
1200	3.90[−2]	5.18[−2]	7.86[−2]	3.87[−3]	2.52[−3]	2.39[−3]	1.69[−3]
1300	4.03[−1]	6.07[−1]	2.67[−2]	4.60[−3]	2.39[−3]	3.01[−3]	1.88[−3]
1400	5.37[0]	3.32[−1]	2.51[−2]	5.06[−3]	3.37[−3]	2.27[−3]	1.70[−3]

W (eV)	80°	90°	100°	110°	130°	150°	SDCS
10	1.66[1]	1.61[1]	1.21[1]	2.72[1]	7.11[0]	2.00[0]	1.36[2]
15	6.40[0]	6.79[0]	4.60[0]	5.87[0]	2.34[0]	9.88[−1]	5.38[1]
20	3.83[0]	3.51[0]	2.71[0]	2.21[0]	1.03[0]	5.52[−1]	2.80[1]
30	2.56[0]	2.10[0]	1.46[0]	7.80[−1]	3.52[−1]	2.27[−1]	1.38[1]
50	1.50[0]	1.12[0]	5.28[−1]	1.72[−1]	7.35[−2]	5.17[−2]	5.77[0]
100	5.50[−1]	1.97[−1]	7.73[−2]	1.56[−2]	1.01[−2]		1.48[0]
200	7.21[−2]	1.29[−2]	5.83[−3]	3.61[−3]	3.66[−3]	3.60[−3]	3.07[−1]
300	3.20[−3]	2.28[−3]	1.78[−3]			2.52[−3]	1.01[−1]
500	1.12[−3]		1.69[−3]		2.71[−3]		4.63[−2]
700		8.20[−4]	1.02[−3]				1.91[−2]
900					1.62[−3]	2.10[−3]	2.84[−2]
1000	4.62[−4]	1.24[−4]		4.57[−4]	1.91[−3]	2.33[−3]	3.57[−2]
1100			9.54[−4]	5.66[−4]	1.45[−3]		5.10[−2]
1200	2.76[−4]		3.56[−4]	2.52[−4]			9.37[−2]
1300	5.92[−4]		7.40[−4]	3.01[−4]		1.86[−3]	2.35[−1]
1400	6.96[−4]	1.83[−4]	6.97[−4]	3.80[−4]	6.66[−4]		5.76[−1]

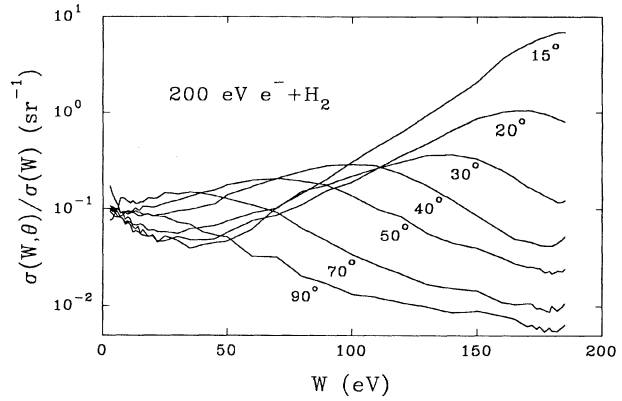

FIG. 7. Ratios of DDCS to SDCS for various angles for 200-eV primary electrons. Note convergence to the value $1/4\pi$ as $W \rightarrow 0$.

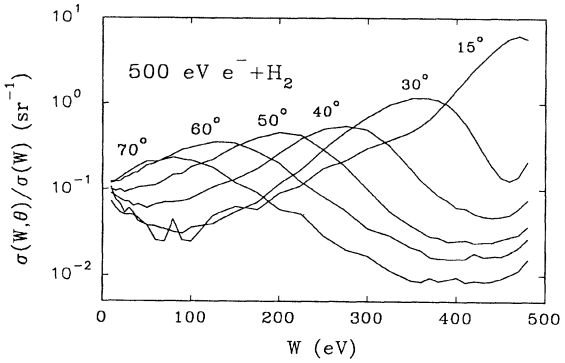

FIG. 8. Same as Fig. 7 for 500-eV primary electrons.

ments on other targets have extended to such high secondary energies, it is difficult to say for sure.

Figure 6 shows the DDCS's for 500 eV as a function of angle compared to those of Opal, Peterson, and Beaty [1] and to the semiempirical model. The general agreement is quite good at the intermediate angles, but there is more divergence at large and small angles. The rising trend of our data at 15° is probably spurious as it is reduced but not completely eliminated by the biasing of the slit after the analyzer described in Sec. IV and in Ref. [9].

It is useful to calculate the ratio of the DDCS to the SDCS. Dividing by the SDCS reduces the large slopes at low and high energies and displays the binary peaks and other features characteristic of each angle more clearly. Such plots appear in Figs. 7 and 8. Equations (5) and (8) of the semiempirical model yield

$$\frac{\sigma(w,t,\theta)}{\sigma(w,t)} = \frac{f_{\mathrm{BE}} + G_4 f_b}{g_{\mathrm{BE}} + G_4 g_b} \ . \tag{21}$$

For $t \gg 1$, this equation may be approximated by

$$\sigma(w,t,\theta)/\sigma(w,t) = f_{\mathrm{BE}}/g_{\mathrm{BE}} \ . \tag{22}$$

Then as $w \rightarrow 0$ the ratio of cross sections described by the model approaches $1/4\pi$, a constant independent of angle. The experimental data tend to converge to that value. The isotropic distribution of very low-energy secondary electrons can be understood from a simple classical picture. The fast primary electron rapidly leaves the collision region after giving a sudden small impulse to the target electron. This slow secondary electron is not necessarily emitted radially and since it has a random distribution of initial positions it has an equal probability of being deflected by the field of the parent ion into any direction. If instead the outgoing electron (primary or secondary) has a large momentum after the collision, its direction is relatively unaffected by the field of the parent ion and it appears at the angle expected for a free-electron target, i.e., it comes at the binary peak angle θ_0 given by Eq. (12). The finite width of the binary peak is caused, of course, by the initial distribution of momentum of the target electron.

VI. CONCLUSIONS

The SDCS's for ejection of electrons by electron impact are well represented by either the BEA or by the semiempirical model. At the minima in the curve where there are small differences in the two representations the experimental values are intermediate between the two. We have shown that for $w \ll t$ a plot of $I\sigma(w,t)/\sigma_{\mathrm{ion}}$ vs $w+1$ yields a universal straight line for all primary energies (provided that $t \gg 1$). This kind of plot should be useful in assessing the accuracy of experimental SDCS data.

The DDCS's are reasonably well represented by the semiempirical model over some ranges of angle and secondary-electron energy, but less well over other ranges. The fit seems to be fairly good near the binary peak but less satisfactory away from it. A larger than expected cross section for angles greater than 90° is suspected to be spurious.

ACKNOWLEDGMENTS

The authors wish to thank George Kerby III for his continuing interest and assistance and Yong-Ki Kim for helpful suggestions. This material is based on work supported by the National Science Foundation under Grants Nos. PHY8701905, PHY9020529, and PHY9119818.

[1] C. B. Opal, W. K. Peterson, and E. C. Beaty, J. Chem. Phys. **55**, 4100 (1971). See also C. B. Opal, E. C. Beaty, and W. K. Peterson, At. Data Nucl. Data Tables **4**, 209 (1972).

[2] T. W. Shyn, W. E. Sharp, and Y.-K. Kim, Phys. Rev. A **24**, 79 (1981).

[3] R. D. DuBois and M. E. Rudd, Phys. Rev. A **17**, 843 (1978).

[4] L. Vriens, Case Stud. At. Phys. **I**, 337 (1969).

[5] M. E. Rudd, Phys. Rev. A **44**, 1644 (1991).

[6] R D. DuBois and M. E. Rudd, J. Phys. B **8**, 1474 (1975).
[7] M. E. Rudd and R. D. DuBois, Phys. Rev. A **16**, 26 (1977).
[8] M. A. Bolorizadeh and M. E. Rudd, Phys. Rev. A **33**, 882 (1986).
[9] K. W. Hollman, G. W. Kerby III, M. E. Rudd, J. H. Miller, and S. T. Manson, Phys. Rev. A **38**, 3299 (1988).
[10] D. Rapp and P. Englander-Golden, J. Chem. Phys. **43**, 4381 (1965).